

Comparison of Ultraviolet B Light-Emitting Diodes with Single or Triple Quantum Wells

Tim Kolbe,* Arne Knauer, Jan Ruschel, Jens Rass, Hyun Kyong Cho, Sylvia Hagedorn, Johannes Glaab, Neysha Lobo Ploch, Sven Einfeldt, and Markus Weyers

Light-emitting diodes (LEDs) with an emission wavelength of 310 nm containing either a single or a triple quantum well are compared regarding their efficiency and long-term stability. In addition, the influence of the thickness of the lower quantum well barrier and the quantum well thickness in single quantum well (SQW) LEDs is investigated. Electroluminescence measurements show a 28% higher initial output power for the SQW LEDs compared with the triple quantum well (TQW) LEDs because of larger spatial overlap of the carriers in the SQW as revealed by electro-optical simulations of the LED heterostructures. However, TQW LEDs show a higher output power than SQW LEDs after 1 h operation under harsh conditions. For SQW LEDs, it is found that for a thicker lower quantum well barrier (65 nm instead of 25 nm) the initial output power decreases by $\approx 15\%$. A thicker SQW (3 nm instead of 1.6 nm) reduces the initial output power by even 45% but increases the lifetime by a factor of 6 which is attributed to reduced Auger recombination from an enhanced spatial separation of electrons and holes in the quantum wells due to the quantum-confined Stark effect.

characteristics of these devices are still low compared with visible LEDs.^[3–5] Today, the best UVB LEDs exhibit an external quantum efficiency in the range of only a few percent.^[6–11]

Optimization of the semiconductor heterostructure is very important to improve the output power, the operating voltage, and the lifetime of UV LEDs. Therefore, we have previously discussed the influence of the n-layer heterostructure design,^[12] the quantum well (QW), and quantum-barrier composition,^[13] the QW width^[14] as well as the electron blocking layer (EBL) design^[15,16] on the emission characteristics and efficiency of triple quantum well (TQW) LEDs in the UVB spectral region. First, investigations on single quantum well (SQW) LEDs have shown that these LEDs are potential candidates for an increase in the output power compared with LEDs with TQWs (see Experimental Section).

In the past, the heterostructure of UVB LEDs was mainly optimized using multiple quantum wells. So far, only a small number of publications on the optimization of SQW UV LEDs can be found, e.g., the variation of the substrate,^[17] the optimization of the buffer layer,^[18] or the optimization of a carrier confinement structure^[19] have been studied. Up to date, a detailed optimization of SQW UV LEDs is missing. In this article, first, the efficiency and the long-term stability of TQW and SQW LEDs with an emission wavelength of 310 nm will be compared. Second, the influence of the QW thickness and the thickness of the lower QW barrier of 310 nm SQW LEDs will be discussed. Simulations of the carrier injection into the active region of the UVB LEDs will be used for interpretation of the experimental data.

1. Introduction

Ultraviolet B (UVB) light-emitting diodes (LEDs) based on the (In)AlGaIn material system must have a high efficiency and a long lifetime to fully exploit their technical potential in applications. These applications include, for example, the curing of polymers, phototherapy, plant growth, and sensing.^[1,2] However, despite the enormous progress that UVB LEDs have made, the performance

Dr. T. Kolbe, Dr. A. Knauer, J. Ruschel, Dr. J. Rass, Dr. H. Kyong Cho, Dr. S. Hagedorn, Dr. J. Glaab, Dr. N. Lobo Ploch, Dr. S. Einfeldt, Prof. M. Weyers
Ferdinand-Braun-Institut gGmbH
Leibniz-Institut für Höchstfrequenztechnik
Gustav-Kirchhoff-Strasse 4, 12489 Berlin, Germany
E-mail: tim.kolbe@fbh-berlin.de

Dr. T. Kolbe, Dr. J. Rass, Dr. N. Lobo Ploch
UVphotonics NT GmbH
Gustav-Kirchhoff-Strasse 4, 12489 Berlin, Germany

 The ORCID identification number(s) for the author(s) of this article can be found under <https://doi.org/10.1002/pssa.202100100>.

© 2021 The Authors. physica status solidi (a) applications and materials science published by Wiley-VCH GmbH. This is an open access article under the terms of the Creative Commons Attribution-NonCommercial-NoDerivs License, which permits use and distribution in any medium, provided the original work is properly cited, the use is non-commercial and no modifications or adaptations are made.

DOI: 10.1002/pssa.202100100

2. Results and Discussion

2.1. Comparison of SQW and TQW LEDs

LEDs with a 25 nm-thick lower quantum well barrier and single or triple 1.6 nm-thick QW are compared. The rest of the LED heterostructure and all growth conditions were kept constant.

Figure 1 shows the normalized optical output power–current density characteristics of the LEDs. Over the whole investigated current density range, the SQW LED shows a higher output power than the TQW LED. At 70 A cm^{-2} , the difference in the average output power is $\approx 28\%$. The inset of Figure 1 shows typical

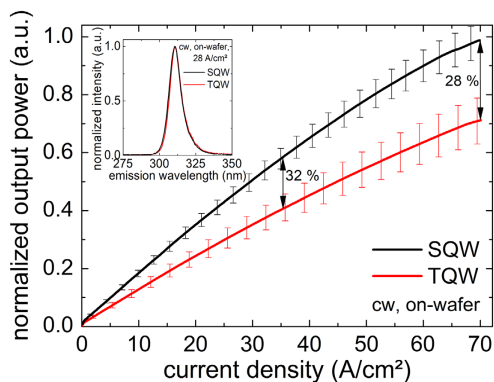


Figure 1. Normalized optical output power–current density characteristic of LEDs with an SQW and a TQW (1.6 nm QW thickness, averaged values with error bars [standard deviation of the mean]). The inset shows typical emission spectra of the LEDs at 20 mA.

emission spectra recorded at 28 A cm^{-2} (20 mA). Both types of LEDs show a single-peak emission with the same peak wavelength of 310 nm and the same full width at half maximum of 9.8 nm. This indicates comparable growth conditions of the SQW and the TQW and of the different quantum wells of the TQW LED.

To explain the experimental data, the carrier injection into the active region has been simulated based on a 1D drift-diffusion model.^[20] A nonradiative carrier lifetime of 3 ns, an electron mobility of $100 \text{ cm}^2 \text{ V}^{-1} \text{ s}^{-1}$, and a hole mobility of $5 \text{ cm}^2 \text{ V}^{-1} \text{ s}^{-1}$ were assumed. **Figure 2** shows the calculated internal quantum efficiency (IQE) as a function of the current density for an SQW and for a TQW LED. The IQE of the SQW LED is higher compared with the TQW LED. However, with increasing current density the difference between both LED types becomes smaller. At 50, 100, and 150 A cm^{-2} , the IQE of the SQW LED is higher than that of the TQW by 37%, 24%, and 18%, respectively. The simulation data from **Figure 2** is in good agreement with the experimental data ($\approx 30\%$ at 50 A cm^{-2} , same trend) from **Figure 1**, assuming that the light extraction efficiency of both sample types is the same.

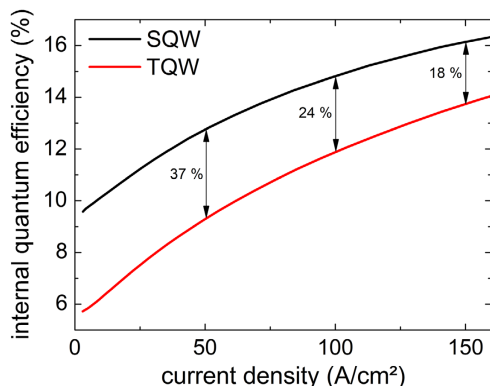


Figure 2. Simulated internal quantum efficiency as a function of the current density of LEDs with an SQW and a TQW (1.6 nm QW thickness), respectively.

Figure 3a,b shows the simulated electron and hole concentration as well as the valence band (VB) and conduction band (CB) edges of the active region of LEDs with a SQW (**Figure 3a**) and a TQW (**Figure 3b**), respectively, at a typical operation current density of 70 A cm^{-2} . Due to the strong piezoelectric fields in the nitride material system,^[21] the VB and CB edges are spatially inclined and electrons and holes are localized on the opposite sides of the QWs. For the SQW LED, high electron and hole concentrations with a large spatial overlap with each other (see gray circle) in the only one quantum well can be observed. For the TQW LED, the distribution of the carriers over the three quantum wells is uneven. In growth direction, the hole concentration is highest in the first well, whereas the electron concentration is highest in the last well. This results in a reduced overall spatial overlap of electrons and holes and in consequence to a 26% reduced radiative recombination of carriers with respect to the SQW LED. Therefore, the IQE and, consequently, the output power are reduced as well for typical operation conditions. However, in addition to the charge carrier distribution, one should consider also another effect that would also lead to a lower efficiency of the TQW LED compared with the SQW LED: the thicker active region of the TQW compared with the SQW could relax more and thus show higher nonradiative recombination.

The lifetime behavior of SQW and TQW LEDs during long-term operation under harsh conditions has been investigated. For this purpose, 15 LEDs per type were operated at a comparably high nominal current density of 134 A cm^{-2} (200 mA) and a heat sink temperature of $55 \text{ }^\circ\text{C}$. Before these measurements starts, incoming component inspection tests show at 0 h and 100 mA a similar voltage of $(7.9 \pm 0.3) \text{ V}$ and an averaged wall plug efficiency of 0.79% and 0.63% for the investigated SQW and MQW LEDs, respectively. The development of the relative output power over the operation time is shown in **Figure 4** together with fits using the model described in the study by Ruschel et al.^[22] It can be seen that the L70 lifetimes (the time within which the output power drops to 70% of the initial value) is about 31 h for the TQW LEDs, but only 1 h for the SQW LED. It seems reasonable to attribute this difference to the different charge carrier distribution in the active region of these LEDs. The optical power of the SQW LED is higher than that of the MQW LED. Assuming that both LEDs differ only in the number of QWs, the overlap of the electron and hole distributions must be larger in the SQW, which is consistent with the results from the simulation. Thus, it can be concluded that a high carrier density in the QWs is possibly related to the faster degradation in optical power. Similar observations were already made by Ruschel et al.,^[22] who found that the L70 lifetime in UVB LEDs is significantly reduced with increasing operation current density. The authors suggested that a high charge carrier density in the active region favors Auger recombination, which results in the generation of hot carriers^[23] with high kinetic energy. These carriers activate point defects acting as centers for nonradiative recombination,^[24] thus reducing the optical power. Therefore, it can be proposed that the SQW LED degrades faster than the TQW LED due to enhanced Auger recombination of carriers resulting from the higher carrier density. Another mechanism which can also explain the faster degradation of the SQW LEDs is the migration of point defects^[25] from the n-contact layer into the active region during the

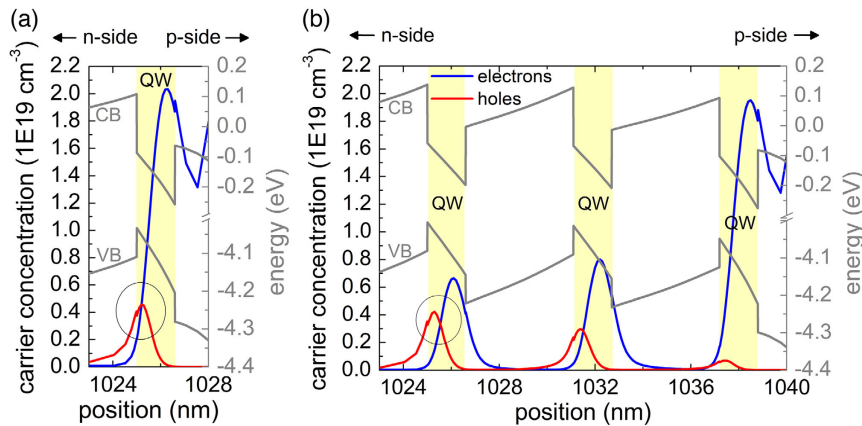


Figure 3. Simulated electron (blue) and hole (red) concentration as well as the energies of the VB and CB edges of the active region of LEDs with a) an SQW and b) a TQW (1.6 nm QW thickness). The simulations were done for a current density of 70 A cm^{-2} .

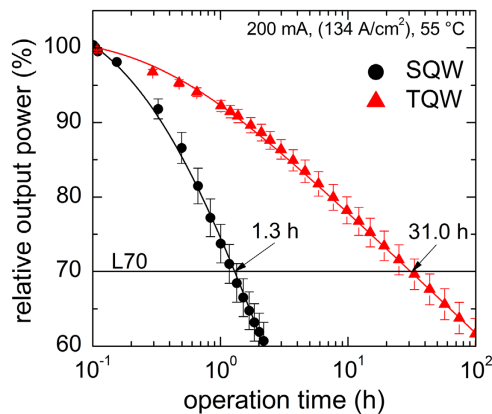


Figure 4. Evolution of the relative output power as a function of the operation time of LEDs with an SQW and a TQW (1.6 nm QW thickness), respectively. The accelerated aging was carried out at a heat sink temperature of 55 °C and a current of 200 mA (134 A cm^{-2}). The symbols and error bars correspond to the mean values and the standard deviation of the mean from 15 nominally identical LEDs of each type. The solid lines are fits using the model described in the study by Ruschel et al.^[22]

operation. If these point defects were acting as non-radiative recombination centers the lifetime of TQW LEDs could be less affected than the lifetime of SQW LEDs because the two additional upper QWs of the TQW have a larger distance to the n-contact layer.

The initially higher output power of the SQW LEDs compared with TQW LEDs is not an advantage in the long run. Due to their different degradation rates, after only 1 h of operation under harsh conditions, the output power of the TQW LEDs is already higher than that of the SQW LEDs. For most applications, TQW LEDs will therefore be preferred. It should be noted that many design parameters of the active region influence the charge carrier distribution and density in the active region, e.g., the number of QWs, their thickness or the doping levels, distances to the n-/p-doped regions, barrier heights, the EBL, and so on. Therefore, all these parameters should also affect the output power and aging behavior.

2.2. Variations in the Active Region of SQW LEDs

The active region of SQW LEDs has been varied to look for further possible improvements in output power and lifetime. At first, the thickness of the lower n-InAlGaN QW barrier (silicon concentration $\approx 2 \times 10^{18} \text{ cm}^{-3}$) was varied between 25 and 65 nm by modifying the growth time. This barrier separates the highly doped n-contact layer (silicon concentration $\approx 1 \times 10^{19} \text{ cm}^{-3}$) from the QW. Its thickness could influence the injection efficiency of electrons into the well and, thus, the efficiency and lifetime of the LED.

Figure 5 shows the output power of SQW LEDs with 25, 45, and 65 nm-thick lower QW barrier measured on-wafer at 20 mA. The highest output power of 1.3 mW is found for the LED with the thinnest lower QW barrier. For thicker barriers, the output power decreases to around 1.1 mW. Simulations indicate a slight decrease in the electron and hole concentrations in the QW if the lower QW barrier becomes thicker (not shown here). This can be attributed to the lower doping level of the lower QW barrier as compared with the n-AlGaN contact layer resulting in a slightly higher potential barrier for the holes at the interface between the active region and the EBL. It should be mentioned, that, however, the operation voltage of all LEDs is almost the same despite the different thickness of the lower QW barrier ($[6.8 \pm 0.2] \text{ V}$ at 20 mA).

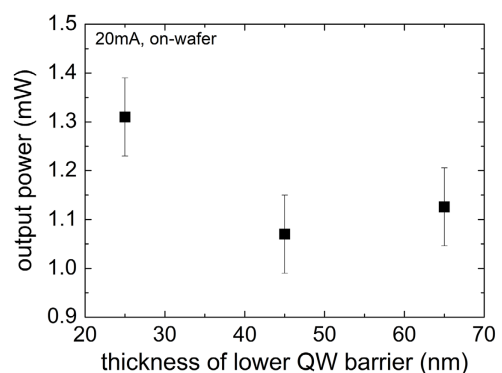


Figure 5. Averaged output power of SQW LEDs (1.6 nm-thick QWs) with lower QW barriers of different thickness measured on-wafer at 20 mA.

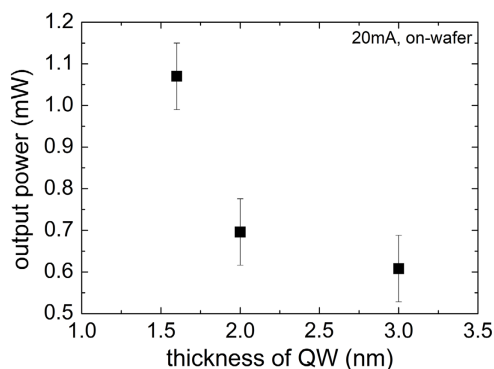


Figure 6. Averaged output power of SQW LEDs (45 nm-thick lower QW barrier) with QWs of different thicknesses measured on-wafer at 20 mA.

In a next step, the thickness of the SQW was increased to lower the charge carrier density in the well. LEDs with a 45 nm-thick lower QW barrier were used. The output power at 20 mA of corresponding LEDs is shown in **Figure 6**. The output power decreases from around 1.1 mW for a thickness of 1.6 nm to 0.6 mW for 3.0 nm. The data suggest that the radiative recombination rate in the SQW decreases with increasing QW thickness which has already been pointed out for example by Hirayama et al.^[26] This can be attributed to an enhanced spatial separation of the electrons and holes in the QW due to the quantum-confined Stark effect. In addition, a thicker QW could also enhance strain relaxation of the active region which could result in the generation of further nonradiative recombination centers and thus in a lower output power. Other effects like a possible increase in the electron and hole concentrations in the active region with increasing QW thickness, which could result from a reduced quantization energy in the QW with a larger thickness (and thus in an enhanced confinement of the carriers in the well), play only a minor role. It should be mentioned that the operation voltage of all LEDs is almost the same despite their different QW thickness ($[7.3 \pm 0.3]$ V).

Selected SQW LEDs with different thicknesses of the QW and the lower QW barrier were stressed to investigate their long-term stability. Once again, harsh stress conditions for an accelerated aging were chosen (heat sink temperature of 55 °C, current of 200 mA [134 A cm^{-2}]). **Table 1** shows the corresponding L70 lifetimes. The increase in the thickness of the lower QW barrier from 25 to 45 nm increases the L70 lifetime by a factor of nearly

Table 1. Averaged output power and L70 lifetime of SQW LEDs with different thicknesses of the lower QW barrier and different QW thicknesses. The accelerated aging was conducted at a heat sink temperature of 55 °C and a current of 200 mA (134 A cm^{-2}). The measurement values correspond to the mean values and the standard deviation of the mean from 15 nominally identical LEDs of each type.

Thickness of lower QW barrier [nm]	Thickness of QW [nm]	Averaged output power @ 20 mA [mW]	L70 lifetime [h]
25	1.6	1.3 ± 0.1	1.3 ± 0.2
45	1.6	1.1 ± 0.1	3.0 ± 0.5
45	3.0	0.6 ± 0.1	18.7 ± 5.0

3 from 1 h to around 3 h. This could be explained by a reduced migration of point defects^[25] from the n-contact layer into the QW during operation because of the thicker lower QW barrier. The thickness of the SQW has an even stronger impact on the lifetime. If the thickness of the QW is increased from 1.6 to 3.0 nm, the L70 lifetime is extended by a factor of 6 to around 19 h. This can be attributed to a lower charge carrier density and the enhanced separation of the electrons and holes in the active region due to the quantum-confined Stark effect which probably reduces the Auger recombination rate, as explained in Section 2.1. However, despite these optimizations, the lifetime of the best SQW LEDs still lags behind that of TQW LEDs, which show a L70 lifetime of 31 h. Furthermore, the initial output power of SQW LEDs with a thick QW is also lower compared with TQW LEDs which is another disadvantage.

3. Conclusions

The performance of TQW and SQW LEDs emitting at 310 nm has been investigated. It could be shown, that design parameters, which influence the charge carrier distribution and concentration in the active region of the LEDs do not only affect the optical output power but also the lifetime of the devices.

SQW LEDs show a higher initial output power than TQW LEDs because of the higher electron and hole concentrations in only one quantum well which results in a larger spatially overlap of both carrier types. Therefore, for typical current densities, the radiative recombination probability in SQW LEDs is increased compared with TQW LEDs. Lifetime measurements show, that after ≈ 1 h of operation under harsh conditions, TQW LEDs have a higher output power and a smaller degradation rate than SQW LEDs. Therefore, for most applications, TQW LEDs would be preferred over SQW LEDs. These optimized TQW LEDs show at moderate current densities extrapolated L70 lifetimes of larger than 10 000 h.

SQW LEDs with the thinnest lower QW barrier (25 nm) show the highest initial output power and the shortest lifetime. An increasing thickness of the lower barrier results in a decreasing initial output power but also in a rising lifetime of the LEDs. An increasing quantum well thickness results in a remarkable decrease in output power but also in an increasing lifetime. All the trends can be attributed to a varying concentration and spatial separation of electrons and holes in the QW due to the quantum-confined Stark effect. A lower charge carrier density and a larger spatial separation of electrons and holes in the active region decrease radiative recombination and thus the initial output power. But at the same time, they could also reduce Auger recombination, so that less energetic carriers are generated, which can activate nonradiative point defects and enhance nonradiative recombination over time.

4. Experimental Section

The 310 nm LEDs were grown on 2 in. sapphire/AlN templates by metal-organic vapor phase epitaxy (MOVPE). Trimethylaluminum, trimethylgallium, triethylgallium, trimethylindium, ammonia, disilane, and bis-cyclopentadienylmagnesium were used as source materials. The templates were grown in a 11 × 2 in. planetary reactor on (00.1) oriented sapphire substrates in a first epitaxy run. They consisted of a 1600 nm AlN

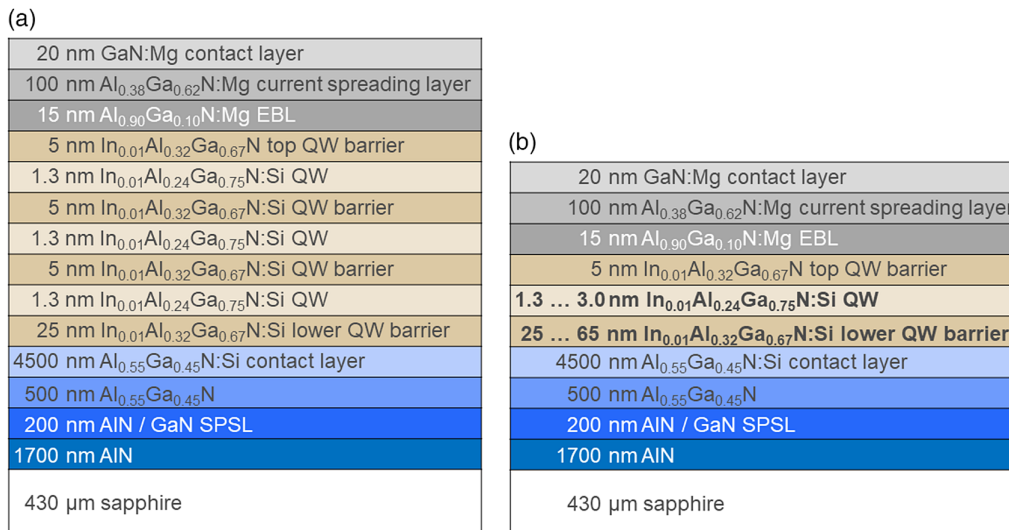


Figure 7. Schematic figure of the investigated a) TWQ and b) SQW LED heterostructure.

layer deposited at elevated temperature. After the template growth, the LED heterostructures were grown in a 6×2 in. close-coupled showerhead reactor. After deposition of a 100 nm-thick AlN base layer, a 200 nm AlN/GaN short period superlattice (SPSL) was grown followed by 500 nm undoped and 4.5 μm silicon-doped Al_{0.55}Ga_{0.45}N contact layer, a single or triple In_{0.01}Al_{0.24}Ga_{0.75}N/In_{0.01}Al_{0.32}Ga_{0.67}N:Si QW active region, a 16 nm-thick magnesium-doped Al_{0.90}Ga_{0.10}N EBL, 100 nm magnesium-doped Al_{0.38}Ga_{0.62}N current spreading layer and a 20 nm-thick heavily magnesium-doped GaN contact cap layer. Schematic figures of the investigated LED heterostructures are shown in **Figure 7**. The AlN base layer on the sapphire/AlN template showed a typical full width at half maximum of the omega X-ray rocking curves of 80 arcsec for the (00.2) reflection and 550 arcsec for the (10.2) reflection. The corresponding threading dislocation density was about $(3\text{--}4) \times 10^9 \text{ cm}^{-2}$.^[27,28] The dislocation density in the active region, determined by counting the dark spot density in monochromatic plan-view cathodoluminescence images of the QW emission was between $(1 \text{ and } 2) \times 10^9 \text{ cm}^{-2}$.^[29] The layer thicknesses were determined by in situ reflectometry, scanning transmission electron microscopy, and scanning electron microscopy measurements on the cross section of the heterostructures. The degree of strain relaxation and layer compositions were determined by high-resolution X-ray diffraction using $\omega\text{--}\omega/2\theta$ reciprocal space maps (RSMs) of the (00.4) and (11.4) reflections in a Malvern PANalytical X'Pert3 system. Thereby, the silicon-doped Al_{0.55}Ga_{0.45}N contact layer showed a typical strain relaxation of 66%. The active region was pseudomorphically grown on the n-Al_{0.55}Ga_{0.45}N contact layer.

In a first step, the performance of LEDs with a TQW (each quantum well 1.6 nm thick, 25 nm lower QW barrier, and 5 nm inner and top QW barrier) and a 1.6 nm-thick SQW (QW barriers like in the TQW LED) was compared. Therefore, the rest of the LED heterostructure and the growth process were kept constant. In a second step, the active region design of the SQW LEDs was varied in two different sample series. In the first series of samples, the thickness of the lower In_{0.01}Al_{0.32}Ga_{0.67}N:Si QW barrier was varied between 25 and 65 nm. The nominal silicon concentration ($2 \times 10^{18} \text{ cm}^{-3}$) of this layer and the rest of the LED heterostructure were kept constant. In a second series, the In_{0.01}Al_{0.24}Ga_{0.75}N quantum well thickness was varied between 1.6 and 3 nm using a 45 nm-thick lower QW barrier.

After MOVPE growth, the samples were annealed in nitrogen ambient to activate the Mg dopants. LEDs were fabricated using standard chip-processing technologies (detailed information can be found in the studies by Rass et al.^[30,31]). Mesa structures were defined by inductively coupled plasma etching to expose the n-AlGaIn surface. Platinum based p-contacts

and vanadium–aluminum based n-contacts were deposited to form the p-electrode and the n-electrode, respectively. The electrical and optical characteristics of the LEDs were measured on-wafer under direct current (DC) injection. For that purpose, the wafers were placed upside up on a sample holder without active cooling. The emission spectra and the optical power versus current ($I\text{--}I$) characteristics were measured by collecting the light emitted through the substrate with an optical fiber spectrometer and a calibrated silicon photodiode, respectively.

In addition, lifetime experiments were conducted using batches of 15 nominally identical LED chips mounted in open AlN cavity packages. For each batch, the 15 chips were selected from various areas of the wafer to account for possible nonuniformities in epitaxial growth or the chip process across the wafer. Each batch was operated at a constant heat sink temperature of 55 °C and a constant current of 200 mA (nominal current density of 134 A cm^{-2}), which are harsher conditions than normal operation to accelerate degradation. Here, the nominal current density is defined as the operation current divided by the p-contact area. The drive voltage and the relative optical power were continuously measured during operation for 100 h. Optical power measurements were carried out using SiC photodiodes.

Acknowledgements

The authors thank C. Neumann and T. Petzke for their technical support in epitaxial growth as well as B. Beidoun and T. T. H. Nguyen for their contributions in the preparation and measurements. This work was partially supported by the German Federal Ministry of Education and Research (BMBF) through the consortium “Advanced UV for Life” under the project contracts 03ZZ0130A, and 03ZZ0134B.

Open access funding enabled and organized by Projekt DEAL.

Conflict of Interest

The authors declare no conflict of interest.

Data Availability Statement

Research data are not shared.

Keywords

Auger recombination, efficiencies, heterostructures, reliabilities, single quantum wells, ultraviolet light-emitting diodes

Received: February 25, 2021

Revised: April 15, 2021

Published online: May 28, 2021

- [1] K. Davitt, Y. Song, W. R. Patterson III, A. Nurmikko, M. Gherasimova, J. Han, Y. Pan, R. G. Chang, *Opt. Express* **2005**, *13*, 9548.
- [2] M. Kneissl, J. Rass, *III-Nitride Ultraviolet Emitters – Technology and Applications*, Springer Series in Materials Science 227, Springer, New York **2016**.
- [3] M. Shatalov, W. Sun, R. Jain, A. Lunev, X. Hu, A. Dobrinsky, Y. Bilenko, J. Yang, G. A. Garrett, L. E. Rodak, M. Wraback, M. Shur, R. Gaska, *Semicond. Sci. Technol.* **2014**, *29*, 084007.
- [4] M. S. Shur, *IEEE Trans. Electron Dev.* **2010**, *57*, 12.
- [5] J.-S. Park, J. K. Kim, J. Cho, T. Y. Seong, *ECS J. Solid State Sci. Technol.* **2017**, *6*, Q42.
- [6] M. Kneissl, T. Kolbe, C. Chua, V. Küller, N. Lobo, J. Stellmach, A. Knauer, H. Rodriguez, S. Einfeldt, Z. Yang, N. M. Johnson, M. Weyers, *Semicond. Sci. Technol.* **2011**, *26*, 014036.
- [7] C. Chu, K. Tian, Y. Zhang, W. Bi, Z.-H. Zhang, *Phys. Status Solidi A* **2019**, *216*, 1800815.
- [8] T. Takano, T. Mino, J. Sakai, N. Noguchi, K. Tsubaki, H. Hirayama, *Appl. Phys. Express* **2017**, *10*, 031002.
- [9] J. Zhang, Y. Gao, L. Zhou, Y.-U. Gil, K.-M. Kim, *Semicond. Sci. Technol.* **2018**, *33*, 07LT01.
- [10] Y. Nagasawa, A. Hirano, *Appl. Sci.* **2018**, *8*, 1264.
- [11] M. Kneissl, T.-Y. Seong, J. Han, H. Amano, *Nat. Photonics* **2019**, *13*, 233.
- [12] A. Knauer, T. Kolbe, J. Rass, H. K. Cho, C. Netzel, S. Hagedorn, N. Lobo Ploch, J. Ruschel, J. Glaab, S. Einfeldt, M. Weyers, *Jpn. J. Appl. Phys.* **2019**, *58*, SCCC02.
- [13] A. Knauer, H. Wenzel, T. Kolbe, S. Einfeldt, M. Weyers, M. Kneissl, G. Tränkle, *Appl. Phys. Lett.* **2008**, *92*, 191912.
- [14] T. Kolbe, T. Sembdner, A. Knauer, V. Küller, H. Rodriguez, S. Einfeldt, P. Vogt, M. Weyers, M. Kneissl, *Phys. Status Solidi A* **2010**, *207*, 2198.
- [15] T. Kolbe, J. Stellmach, F. Mehnke, M.-A. Rothe, V. Küller, A. Knauer, S. Einfeldt, T. Wernicke, M. Weyers, M. Kneissl, *Phys. Status Solidi A* **2016**, *213*, 210.
- [16] T. Kolbe, A. Knauer, J. Rass, H. K. Cho, S. Hagedorn, S. Einfeldt, M. Kneissl, M. Weyers, *Materials* **2017**, *10*, 1396.
- [17] T. Mukai, S. Nakamura, *Jpn. J. Appl. Phys.* **1999**, *38*, 5735.
- [18] T. Nishida, T. Ban, N. Kobayashi, *Jpn. J. Appl. Phys.* **2003**, *42*, 2273.
- [19] T. Nishida, H. Saito, N. Kobayashi, *Appl. Phys. Lett.* **2001**, *78*, 3927.
- [20] *Simulations are Based on the Software Package SiLENSe*, STR Group, Ltd.
- [21] F. Bernardini, V. Fiorentini, *Appl. Phys. Lett.* **2002**, *80*, 4145.
- [22] J. Ruschel, J. Glaab, B. Beidoun, N. Lobo Ploch, J. Rass, T. Kolbe, A. Knauer, M. Weyers, S. Einfeldt, M. Kneissl, *Photonics Res.* **2019**, *7*, B36.
- [23] J. Iveland, L. Martinelli, J. Peretti, J. S. Speck, C. Weisbuch, *Phys. Rev. Lett.* **2013**, *110*, 177406.
- [24] J. Glaab, J. Ruschel, T. Kolbe, A. Knauer, J. Rass, H. C. Cho, N. Lobo Ploch, S. Kreuzmann, S. Einfeldt, M. Weyers, M. Kneissl, *IEEE Photon. Technol. Lett.* **2019**, *31*, 529.
- [25] Z. Ma, A. Almalki, X. Yang, X. Wu, X. Xi, J. Li, S. Lin, X. Li, S. Alotaibi, M. Al huwayz, M. Henini, L. Zhao, *J. Alloys Compd.* **2020**, *845*, 156177.
- [26] H. Hirayama, Y. Enomoto, A. Kinoshita, A. Hirata, Y. Aoyagi, *Appl. Phys. Lett.* **2002**, *80*, 37.
- [27] T. Metzger, R. Höppler, E. Born, O. Ambacher, M. Stutzmann, R. Stömmmer, M. Schuster, H. Göbel, S. Christiansen, M. Albrecht, H. P. Strunk, *Philos. Mag. A* **1998**, *77*, 1013.
- [28] H. Heinke, V. Kirchner, S. Einfeldt, D. Hommel, *Phys. Status Solidi A* **1999**, *176*, 391.
- [29] T. Kolbe, A. Knauer, J. Enslin, S. Hagedorn, A. Mogilatenko, T. Wernicke, M. Kneissl, M. Weyers, *J. Cryst. Growth* **2019**, *526*, 125241.
- [30] J. Rass, T. Kolbe, N. Lobo-Ploch, T. Wernicke, F. Mehnke, Ch Kuhn, J. Enslin, M. Guttmann, Ch Reich, A. Mogilatenko, J. Glaab, Ch Stoelmacker, M. Lapeyrade, S. Einfeldt, M. Weyers, M. Kneissl, *Proc. SPIE* **2015**, *9363*, 93631K.
- [31] J. Rass, J. Ruschel, J. Glaab, I. Ostermay, S. Einfeldt, *IEEE Photon. Technol. Lett.* **2020**, *32*, 1007.